Article

Cell Reports

Dissociation of Rad51 Presynaptic Complexes and Heteroduplex DNA Joints by Tandem Assemblies of Srs2

Graphical Abstract

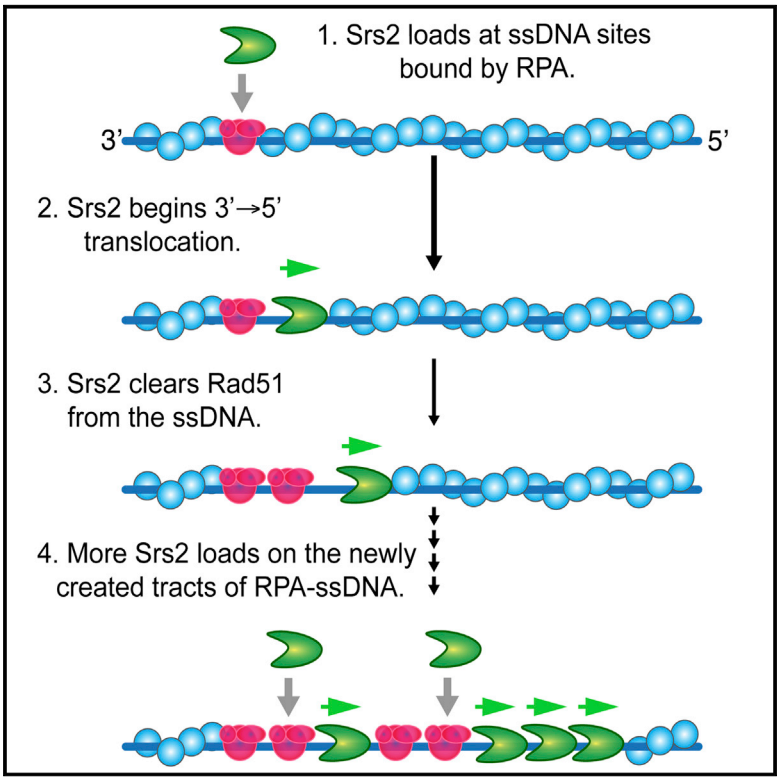

Highlights

- Srs2 is visualized in real time as it translocates on Rad51-ssDNA
- Srs2 rapidly strips Rad51 from ssDNA
- Srs2 loads preferentially at RPA clusters embedded between Rad51 filaments
- Srs2 rapidly disrupts small heteroduplex DNA joints bound to Rad51 filaments

Authors

Kyle Kaniecki, Luisina De Tullio, Bryan Gibb, Youngho Kwon, Patrick Sung, Eric C. Greene

Correspondence

ecg2108@cumc.columbia.edu

In Brief

Kaniecki et al. develop a single-molecule assay for directly visualizing the behavior of the yeast helicase Srs2 as it acts upon single-stranded DNA (ssDNA) bound by the Rad51 recombinase. These experiments lead to a model describing the recruitment and regulation of Srs2 as it acts upon homologous recombination intermediates.

Kaniecki et al., 2017, Cell Reports *21*, 3166–3177
December 12, 2017
https://doi.org/10.1016/j.celrep.2017.11.047

CellPress

OPEN ACCESS
CellPress

Cell Reports
Article

Dissociation of Rad51 Presynaptic Complexes and Heteroduplex DNA Joints by Tandem Assemblies of Srs2

Kyle Kaniecki,[1] Luisina De Tullio,[2,3] Bryan Gibb,[2,5] Youngho Kwon,[4] Patrick Sung,[4] and Eric C. Greene[2,6,*]
[1]Department of Genetics & Development, Columbia University, New York, NY 10032, USA
[2]Department of Biochemistry & Molecular Biophysics, Columbia University, New York, NY 10032, USA
[3]Centro de Investigaciones en Química Biológica de Córdoba (CIQUIBIC), CONICET, Departamento de Química Biológica, Facultad de Ciencias Químicas, Universidad Nacional de Córdoba, Ciudad Universitaria, Córdoba, X5000 HUA, Argentina
[4]Department of Molecular Biophysics and Biochemistry, Yale University School of Medicine, New Haven, CT 06510, USA
[5]Present address: Department of Life Sciences, Theobald Science Center, Room 423, New York Institute of Technology, Old Westbury, NY 11568-8000, USA
[6]Lead Contact
*Correspondence: ecg2108@cumc.columbia.edu
https://doi.org/10.1016/j.celrep.2017.11.047

SUMMARY

Srs2 is a superfamily 1 (SF1) helicase and antirecombinase that is required for genome integrity. However, the mechanisms that regulate Srs2 remain poorly understood. Here, we visualize Srs2 as it acts upon single-stranded DNA (ssDNA) bound by the Rad51 recombinase. We demonstrate that Srs2 is a processive translocase capable of stripping thousands of Rad51 molecules from ssDNA at a rate of ~50 monomers/s. We show that Srs2 is recruited to RPA clusters embedded between Rad51 filaments and that multimeric arrays of Srs2 assemble during translocation on ssDNA through a mechanism involving iterative Srs2 loading events at sites cleared of Rad51. We also demonstrate that Srs2 acts on heteroduplex DNA joints through two alternative pathways, both of which result in rapid disruption of the heteroduplex intermediate. On the basis of these findings, we present a model describing the recruitment and regulation of Srs2 as it acts upon homologous recombination intermediates.

INTRODUCTION

Homologous recombination (HR) allows the exchange of genetic information between two different DNA molecules of identical or nearly identical sequence composition and is a driving force in evolution. HR contributes to DNA double-strand break (DSB) repair (Pâques and Haber, 1999), the rescue of stalled or collapsed replication forks (Symington et al., 2014), chromosomal rearrangements (Mehta and Haber, 2014), and meiosis (Hunter, 2015).

HR is promoted by the *RAD52* epistasis group of genes, which were originally identified in *Saccharomyces cerevisiae* as mutants defective in DNA repair (Pâques and Haber, 1999; Symington et al., 2014). During HR, single-stranded DNA (ssDNA), derived from the nucleolytic processing of a DSB or collapsed replication fork, is quickly bound by RPA (replication protein A), which is a conserved heterotrimeric eukaryotic protein complex that removes ssDNA secondary structure, protects ssDNA from nucleolytic degradation, and serves as a platform from DNA damage signaling (Chen and Wold, 2014). With the aid of Rad52, RPA is replaced by the ATP-dependent DNA-binding protein Rad51, which forms an extended right-handed helical filament on the ssDNA, and the resulting nucleoprotein filament is referred to as the presynaptic complex (Kowalczykowski, 2015). Pairing of the presynaptic complex with a homologous double-stranded DNA (dsDNA) template results in displacement of the non-complementary strand from the duplex to generate a D-loop (Kowalczykowski, 2015). The resulting intermediate can be processed via one of several alternative pathways, any of which can allow the repair of the DSB using information derived from the donor template (Pâques and Haber, 1999; Symington et al., 2014).

Specialized DNA helicases play crucial roles in regulating recombination and do so by dismantling recombination intermediates (Bernstein et al., 2010; Branzei and Szakal, 2017; Brosh, 2013; Symington and Heyer, 2006). Highlighting the importance of these enzymes, mutations in human HR helicases that regulate HR cause diseases such as Rothmund-Thompson syndrome and Fanconi Anemia, which are characterized by genome instability and increased incidence of cancer (Brosh, 2013). Srs2 is considered a proto-typical antirecombinase because of its well-characterized ability to remove Rad51 from ssDNA (Antony et al., 2009; Krejci et al., 2003; Marini and Krejci, 2010; Niu and Klein, 2017; Qiu et al., 2013; Sasanuma et al., 2013; Vasianovich et al., 2017; Veaute et al., 2003). Deletion of the *SRS2* gene results in an increase in recombination frequency, and its importance is further revealed in *srs2Δ sgs1Δ* and *srs2Δ rad54Δ* double mutants, which have a synthetic lethal phenotype due to the accumulation of toxic recombination intermediates (Ira et al., 2003; Klein, 2001). Srs2 is homologous to the bacterial UvrD, PcrA, and Rep helicases (Marini and Krejci, 2010; Niu and Klein, 2017). Human homologs of Srs2 have yet to be identified, although mammalian FBH1 is a potential candidate, and FBH1

can also remove Rad51 from ssDNA (Simandlova et al., 2013). A growing body of evidence suggests that similar antirecombinase regulatory roles might be filled by other helicases, including RECQ1, RECQ5, BLM (Sgs1 in yeast), FANCM (Mph1 in yeast), FANCJ, and RTEL1 (Bernstein et al., 2010; Branzei and Szakal, 2017; Brosh, 2013; Heyer et al., 2010).

Here, we visualized single *S. cerevisiae* Srs2 complexes in real time as they act upon long Rad51-ssDNA substrates resembling physiological presynaptic complexes. We show that Srs2 acts as a processive 3′→5′ ssDNA motor protein. These highly processive complexes are composed of multimeric Srs2 assemblies, which act collectively during disruption of the Rad51 presynaptic complex. Our work also reveals that Srs2 preferentially initiates translocation at clusters of RPA embedded between Rad51 filaments, rather than from within the Rad51 filaments themselves. We show that the Rad51 interaction domain is required primarily for Srs2 recruitment to the presynaptic complex, suggesting that this domain may be involved in initial binding to RPA-ssDNA. Interestingly, an Srs2 mutant lacking this domain is compromised for initial loading, but once bound, it can still efficiently translocate and remove Rad51 from the ssDNA. Finally, we demonstrate that Srs2 can act upon heteroduplex DNA joints though either collisional encounters or direct recruitment. The most prevalent outcome in both scenarios is rapid displacement of the heteroduplex DNA joint. On the basis of these results, we present models for Srs2 recruitment and action in dismantling early recombination intermediates.

RESULTS

Disruption of Rad51-ssDNA Filaments by Srs2

S. cerevisiae Srs2 contains a core superfamily 1 (SF1) helicase domain that is homologous to the bacterial helicase UvrD, a C-terminal region responsible for interactions with Rad51, and a second C-terminal domain that mediates protein-protein interactions and is a target for post-translational modifications (Figure S1A) (Niu and Klein, 2017; Sasanuma et al., 2013). For our experiments, we used Srs2 preparations that were either unlabeled or tagged at the N terminus with either GFP or mCherry, as indicated. This labeling strategy was selected because N-terminal GFP-Srs2 fusion constructs are functional *in vivo* (Burgess et al., 2009). Full-length Srs2 is prone to aggregation, so unless stated otherwise, all constructs were truncated at amino acid 898, yielding $Srs2^{898}$. Previous studies have shown that $Srs2^{898}$ is proficient in ATP hydrolysis and in the disruption of Rad51-ssDNA filaments (Antony et al., 2009; Colavito et al., 2009; Qiu et al., 2013). We also prepared $Srs2^{K41A}$, which is defective in ATP hydrolysis (Krejci et al., 2004), and the truncation mutants $Srs2^{860}$ and $Srs2^{\Delta 875–902}$, which lack the Rad51 interaction domain (Antony et al., 2009; Colavito et al., 2009). The different purified forms of Srs2 were all tested for ATP hydrolysis activity (Figures S1B and S1C).

We have previously used double-tethered ssDNA curtains and total internal reflection fluorescence microscopy (TIRFM) to visualize the behaviors of Srs2 on RPA-coated ssDNA in the presence and absence of Rad52 (De Tullio et al., 2017). Here, we use single- and double-tethered ssDNA curtains to visualize the movement of Srs2 on Rad51-coated ssDNA (Figures 1A, 1B, and S2A). Presynaptic complexes were prepared using wild-type (WT) *S. cerevisiae* Rad51, as described (Lee et al., 2015; Qi et al., 2015). Rad51 was not fluorescently labeled; instead, the assembly and disassembly of the presynaptic complex was assessed by monitoring the binding of GFP-tagged RPA. Once assembled, the Rad51 filaments remain intact for hours in the presence of ATP (Qi et al., 2015).

To determine whether Srs2 could remove Rad51 from the ssDNA, we injected unlabeled $Srs2^{898}$ in 150 μL of buffer containing 2 mM ATP and 100 pM GFP-RPA. Reactions were observed under constant buffer flow (0.2 mL/min), and Srs2 that did not bind during the initial sample injection was flushed away by buffer flow, so the resulting observations only report the behaviors of Srs2 proteins that bind to the RPA-ssDNA during a time window of ~45 s. This strategy was necessary to help minimize overlapping Srs2 binding and translocation events (see below). Under these conditions, we observed extensive Srs2-dependent removal of Rad51 from the ssDNA, as evidenced by the reappearance of GFP-RPA (Figures 1C and S2B; Movie S1). Rad51 removal did not occur when the ATPase defective $Srs2^{K41A}$ mutant protein was tested, confirming that the observed activity required ATP hydrolysis by Srs2 (Figure S3). Moreover, inspection of the kymographs revealed that GFP-RPA reappeared in distinctive wedge-shaped patterns (Figures 1C, S2B, and S3). These patterns suggested that Rad51 removal stemmed from the 3′→5′ motor activity of Srs2, with each track of GFP-RPA resulting from the processive translocation of Srs2 along the ssDNA.

We conducted two-color experiments using GFP-Srs2 and mCherry-RPA to validate the expectation that Srs2 was positioned at the leading 5′ edge of each growing tract of GFP-RPA. As predicted, GFP-Srs2 could be seen translocating in the 3′→5′ direction along the presynaptic complexes, leaving behind extended tracks of mCherry-RPA on the ssDNA (Figures 1D and S2C; Movies S2 and S3). Similar results were obtained in two-color experiments using mCherry-Srs2 and GFP-RPA (see below). Experiments using GFP-$Srs2^{K41A}$ revealed that GFP-$Srs2^{K41A}$ bound to the Rad51-ssDNA filaments but was unable to initiate translocation. These findings provide further evidence that Srs2 movement dependent upon ATP hydrolysis.

Analysis of the GFP-RPA tracks yielded an apparent velocity for unlabeled Srs2 on Rad51 filaments of 142 ± 56 nt/s. Moreover, Srs2 was remarkably processive, with the observed complexes traveling an average distance of 20,800 ± 1,100 nt (n = 420) before stopping (Figures 1E and 1F). The apparent velocity and processivity values for GFP-Srs2 were 142 ± 77 nt/s and 18,500 ± 650 nt (n = 798), respectively (Figures 1G and 1H; Table S1). In all cases, the movement of Srs2 occurred in the 3′→5′ direction. We conclude that *S. cerevisiae* Srs2 is a highly processive ssDNA translocase capable of rapidly stripping Rad51 from the presynaptic complex.

Srs2 Is Recruited to RPA Clusters within the Presynaptic Complex

It has remained unknown how Srs2 is recruited to recombination intermediates. To address this question, we next mapped the

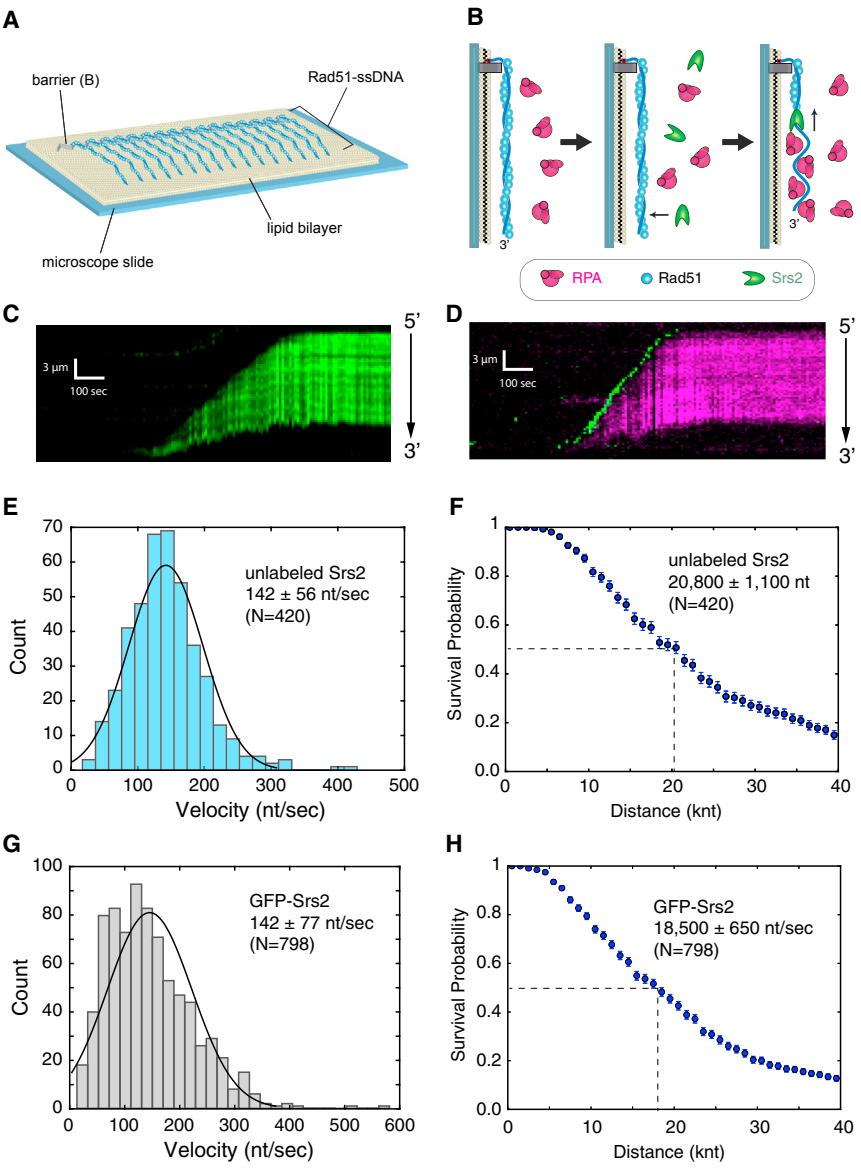

Figure 1. ssDNA Curtain Assays for Srs2 Translocation

For a Figure360 author presentation of Figure 1, see the figure legend at https://doi.org/10.1016/j.celrep.2017.11.047. Figure360▷

(A and B) Schematic of a single-tethered ssDNA curtain (A) and cartoon depiction of Rad51 displacement from ssDNA by Srs2 followed by the binding of RPA (B).

(C) Kymograph showing unlabeled Srs2^{898} removing unlabeled Rad51 from a single-tethered ssDNA molecule; Srs2-mediated Rad51 displacement is revealed by the binding of GFP-RPA (green).

(D) Kymograph showing GFP-Srs2^{898} (green) removing unlabeled Rad51 from a single-tethered ssDNA molecule; Rad51 displacement is revealed by the binding of mCherry-RPA (magenta).

(E and F) Velocity distribution (E) and survival probability (F) of unlabeled Srs2^{898} acting on Rad51-ssDNA.

(G and H) Velocity distribution (G) and survival probability (H) of GFP-Srs2^{898} acting on Rad51-ssDNA.

Dashed lines in (F) and (H) highlight the values at which half of the complexes stop translocating. Error bars in the survival probability plots represent SD calculated from bootstrap analysis.

locations at which Srs2 bound to the presynaptic complexes. The initial Srs2 binding positions appeared randomly distributed along the ssDNA, with a moderate preference for regions closer to the 3′ end of the ssDNA (Figure 2A). The Rad51 filaments in our assays are not contiguous but instead contain short clusters of RPA that were also randomly distributed along the length of the presynaptic complex (Figures 2B and 2C) (Gibb et al., 2014). On the basis of measurements of the cumulative GFP-RPA signal before and after presynaptic complex assembly, the remaining RPA clusters constitute ~2%–5% of the total RPA that was present on the ssDNA prior to Rad51 binding, and the majority of the ssDNA (~95%–98%) is bound by Rad51 (Gibb et al., 2014). Comparison of all Srs2 initiation sites with the entire population of RPA cluster distributions revealed no obvious correlation (cf. Figures 2A and 2B). However, when examined on an individual basis, Srs2 had a marked preference for initiating translocation at sites that coincided with RPA (Figure 2C). We observed that 54% of the Srs2 recruitment events occurred at these RPA clusters, even though these RPA clusters make up only a very small fraction (~2%–5%) of the total ssDNA present (Figure 2D). These values suggest a ~20- to ~60-fold greater likelihood for Srs2 to initiate translocation at an RPA cluster relative to locations at which we detect no RPA. Importantly, the remaining Srs2 recruitment events may also be occurring at RPA clusters that are either too small to detect or may have been photo-bleached over the timescales of our measurements. These results were further validated by examining the binding locations of GFP-Srs2^{K41A} on presynaptic complexes prepared with mCherry-RPA and dark Rad51, which revealed that GFP-Srs2^{K41A} had a strong preference for binding to mCherry-RPA (Figures 2E and 2F). Taken together, these findings support a model in which Srs2 is recruited to small clusters of RPA embedded within the Rad51 presynaptic complex.

Tandem Assemblies of Srs2 Promote Efficient Rad51 Disruption

Interestingly, our data hinted at the possibility that the processive disruption of Rad51 filaments observed in our assays may involve more than just one Srs2 molecule. Specifically, in experiments using 100 pM Srs2, we observed highly processive translocation activity (Figure 3A). However, at lower Srs2

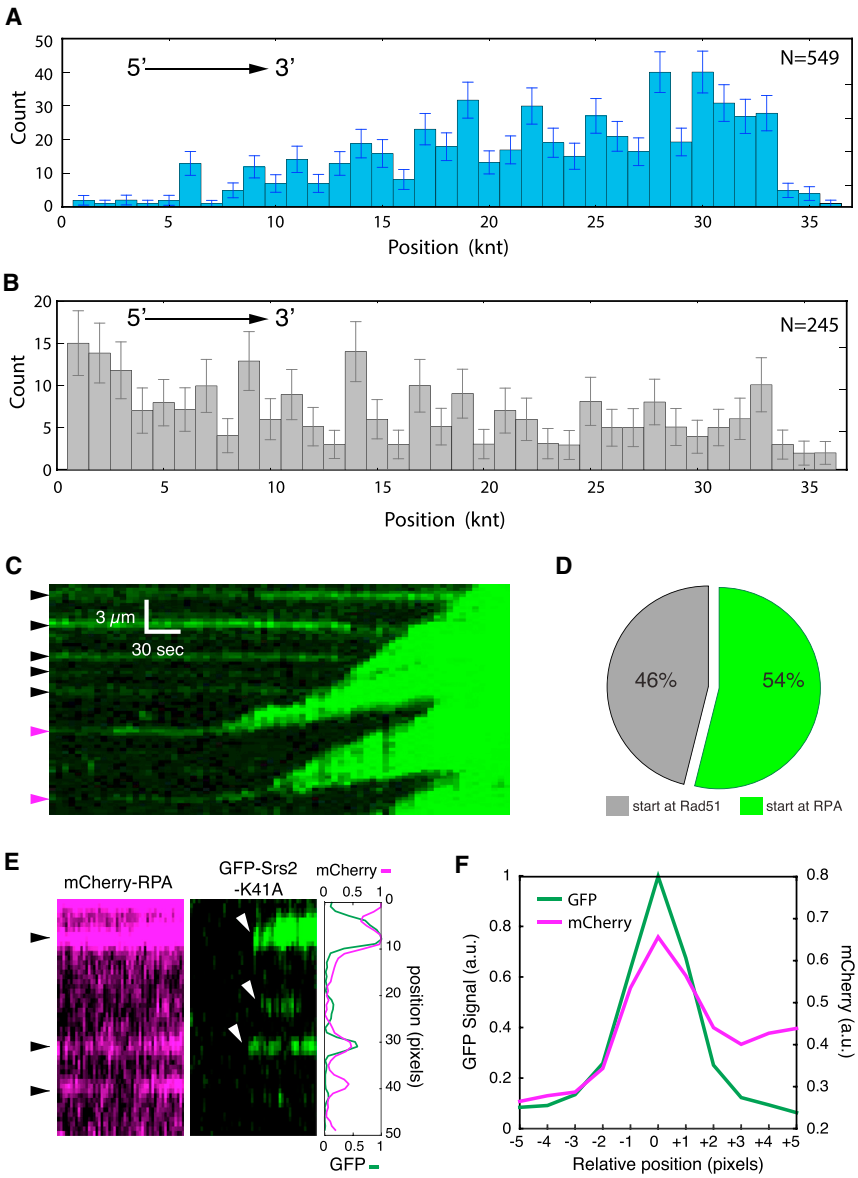

Figure 2. Srs2 Is Preferentially Targeted to RPA Clusters Embedded within the Rad51 Presynaptic Complex

(A and B) Distribution of initial Srs2 binding sites (A) and distribution of RPA clusters embedded within the Rad51 presynaptic complex (B); error bars represent SD calculated by bootstrap analysis.

(C and D) Kymographs showing (C) unlabeled $Srs2^{898}$ translocation beginning from GFP-RPA clusters and (D) pie chart displaying the fraction of Srs2 initiation events that coincided with visible RPA clusters.

(E) Kymographs and line plot showing the association of GFP-Srs2 K41A with mCherry-RPA.

(F) Plot showing the relative GFP-Srs2 K41A and mCherry-RPA signal distributions (n = 67).

concentrations (10 pM), we observed mostly short patches of Rad51 removed from the ssDNA (Figure 3A), and the apparent velocity also increased with Srs2 concentration (Figure 3B). These results suggested that at low concentrations Srs2 was less able to catalyze the highly processive filament disruption.

We often observed fluorescent Srs2 molecules colliding with one another while stripping Rad51 from ssDNA or larger Srs2 complexes separating into smaller independent units, suggesting that assemblies of Srs2 might be traveling along the same ssDNA molecules. Moreover, we also often observed multiple Srs2 binding and translocation events on the same ssDNA molecule, especially over regions of the ssDNA that had already been cleared of Rad51 (Figure 3C; Movie S4), consistent with the notion that Srs2 binds preferentially to RPA-ssDNA relative to Rad51-ssDNA. Interestingly, the trailing Srs2 complexes traveling along RPA-ssDNA often caught up to and merged with the leading Srs2 complexes that are at the 3′ edge of the Rad51 filament. Examples of these mergers were especially evident in cases in which the leading Srs2 displayed fortuitous reduction in velocity (Figure 3C).

Visual inspection of the GFP-Srs2 trajectories also suggested that these complexes were much brighter than might be expected for a single GFP molecule. To validate this interpretation, we used 561 nm laser illumination to first identify tracts of Rad51 that were being dismantled by GFP-Srs2 (100 pM) on the basis of the appearance of mCherry-RPA (Figure 3D). We then quickly viewed the sample with high-intensity 488 nm laser illumination while continuously imaging the GFP-Srs2 signal (Figure 3D). As expected, GFP-Srs2 was located at the leading edges of the growing tracts of mCherry-RPA, and the GFP signal quickly photobleached under these conditions, allowing us to estimate the number of GFP molecules present in the Srs2 complexes on the basis of the number of photo-bleaching steps (Figure 3D). These experiments confirmed that the majority of the GFP-Srs2 complexes displayed multiple photo-bleaching steps, with ~97% of the Srs2 complexes exhibiting two or more bleaching steps (n = 84 of 97) and ~44% exhibiting at least four bleaching steps (n = 38 of 97) (Figure 3E).

Finally, we performed two-color mixing experiments using a combination of GFP-Srs2 and mCherry-Srs2. If Srs2 acted as monomeric units during while disrupting the Rad51 filaments, then GFP- and mCherry-Srs2 should appear as separate entities on the ssDNA. However, if Srs2 multimers were responsible for disrupting the Rad51 filaments, then the fluorescence signals from GFP- and mCherry-Srs2 should overlap on the ssDNA. Consistent with this latter interpretation, when GFP-Srs2 (50 pM) and mCherry-Srs2 (50 pM) were pre-mixed and injected into the sample chamber, only ~5% of the observed signals

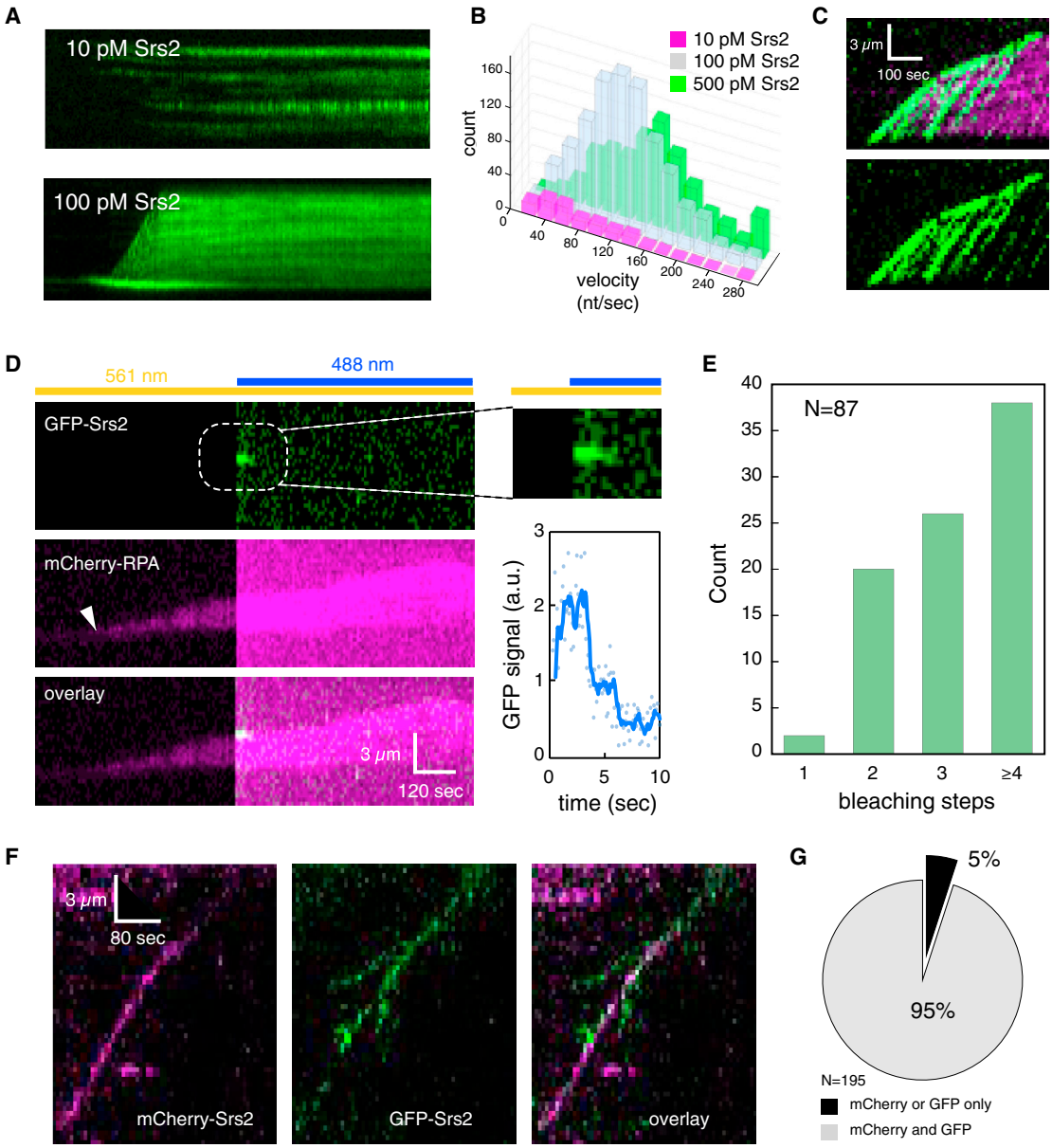

Figure 3. Srs2 Forms Multimeric Complexes during Processive Translocation

(A) Kymographs showing the typical behavior of Srs2^{898} at 10 pM and 100 pM, as indicated.

(B) Velocity distribution profiles for experiments conducted at 10, 100, or 500 pM Srs2^{898}.

(C) Kymograph highlighting an example of numerous Srs2 merging events.

(D) Kymographs and graph showing photo-bleaching step measurements used to confirm that GFP-Srs2^{898} was not acting as a monomer during processive translocation. Orange and blue lines indicate when the sample was being illuminated with the 561 nm and 488 nm lasers, respectively.

(E) Distribution of different bleaching steps measured for translocating GFP-Srs2^{898} complexes.

(F and G) Example of kymograph showing a two-color mixing experiment with GFP-Srs2^{898} and mCherry-Srs2^{898} (F) and fraction of complexes that contained overlapping GFP and mCherry fluorescence (G).

could be ascribed to only one color (n = 10 of 195), whereas ~95% of the observed complexes (n = 185 of 195) contained overlapping GFP and mCherry signals (Figures 3F and 3G). These observations all support the conclusion that the highly processive Srs2 complexes observed in our assays were composed of multiple Srs2 molecules traveling together along the ssDNA.

The Rad51 Interaction Domain Is Required for Srs2 Loading

Efficient removal of Rad51 from ssDNA requires a direct contact between Rad51 and Srs2 (Figure S1A) (Antony et al., 2009; Colavito et al., 2009). *In vitro* studies have shown that an srs2 mutant (Srs2^{860}) lacking these amino acids cannot

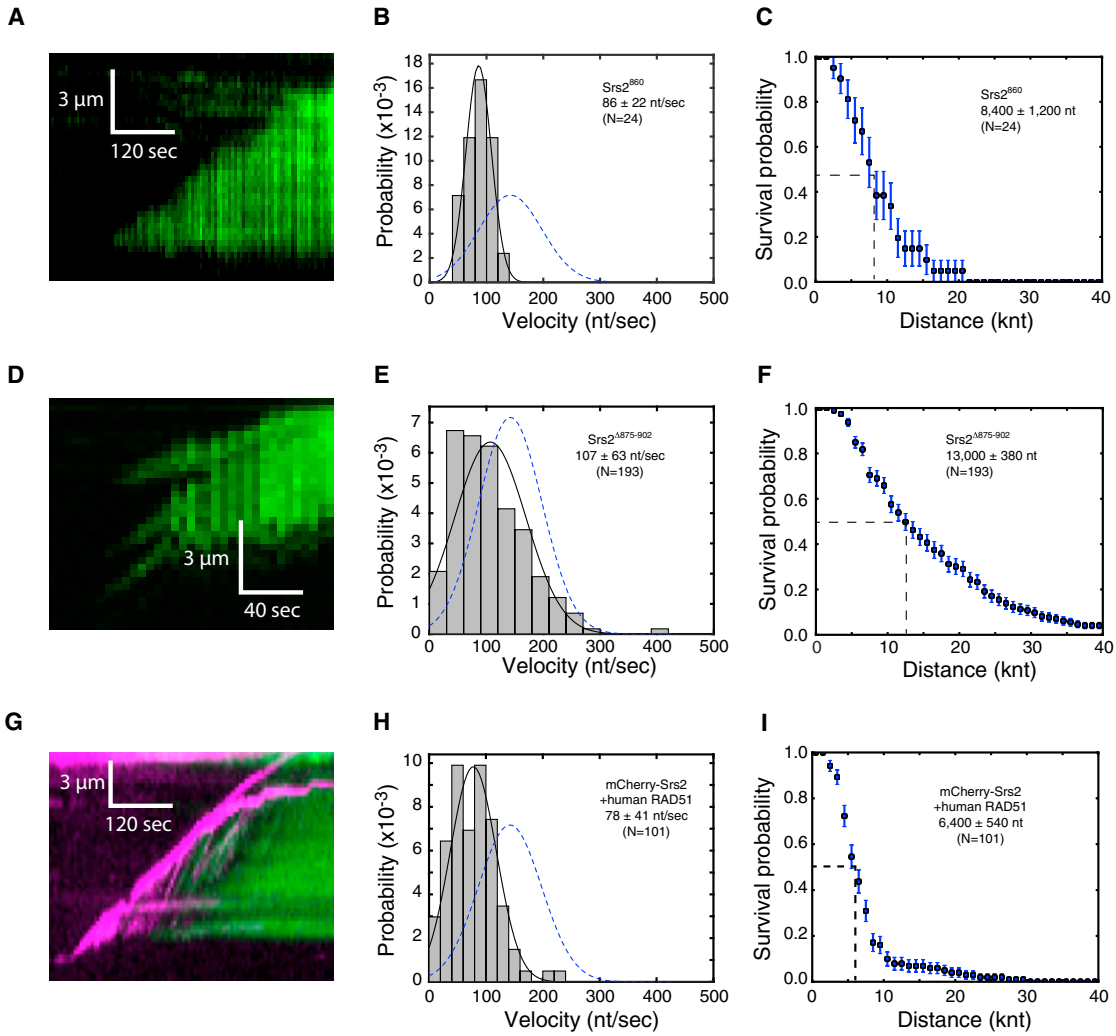

Figure 4. Srs2 Mutants that Affect Rad51 Clearance

(A–C) Kymograph (A), velocity distribution (B), and survival probability (C) for $Srs2^{860}$.

(D–F) Kymograph (D), velocity distribution (E), and survival probability (F) for $Srs2^{\Delta 875–902}$.

(G–I) Kymograph (G), velocity distribution (H), and survival probability (I) for *S. cerevisiae* mCherry-$Srs2^{898}$ acting on ssDNA bound by human RAD51.

Error bars for the survival probability plots represent SD calculated by bootstrap analysis. The velocity distributions in (B), (E), and (H) are superimposed on the Gaussian fit (blue dashed line) for the velocity distribution of unlabeled Srs2 taken from Figure 1E.

interact with Rad51 and also showed greatly diminished ability to disrupt Rad51 filaments (Antony et al., 2009). However, these *in vitro* studies have shown that the interaction defective $Srs2^{860}$ mutant protein has residual activity in Rad51-ssDNA filament disruption, and overexpression of this $Srs2^{860}$ mutant can provide some biological activity (Antony et al., 2009; Colavito et al., 2009). We considered two possibilities for the reduced displacement of Rad51 from ssDNA upon deletion of the Rad51 interaction domain from Srs2: (1) it could attenuate initial association of Srs2 with the Rad51-ssDNA filament, or (2) it might reduce Srs2 processivity, velocity, or both. To distinguish between these models, we assessed the ability of the C-terminally truncated GFP-$Srs2^{860}$ to dismantle Rad51 filaments. These assays revealed that most of the Rad51 filaments (~98%) remained fully intact upon injection of $Srs2^{860}$, confirming that truncation of the Srs2 C terminus greatly diminishes its ability to disrupt the Rad51 filaments. Remarkably, there were a few examples (24 total) of Rad51 filaments being dismantled by $Srs2^{860}$ (Figure 4A). These rare $Srs2^{860}$ translocation events were ~40% slower than reactions with $Srs2^{898}$, exhibiting a rate of 86 ± 22 nt/s (n = 24) (Figure 4B; Table S1). Although $Srs2^{860}$ was not as processive as $Srs2^{898}$, the mutant protein still traveled an average distance of 8,400 ± 1,200 nucleotides before stopping (Figure 4C). We next tested $Srs2^{\Delta 875–902}$, which lacks the Rad51 interaction domain, but retains all of the remaining C-terminal amino acids (Colavito et al., 2009). Interestingly, we were able to observe more translocation events for $Srs2^{\Delta 875–902}$ compared with

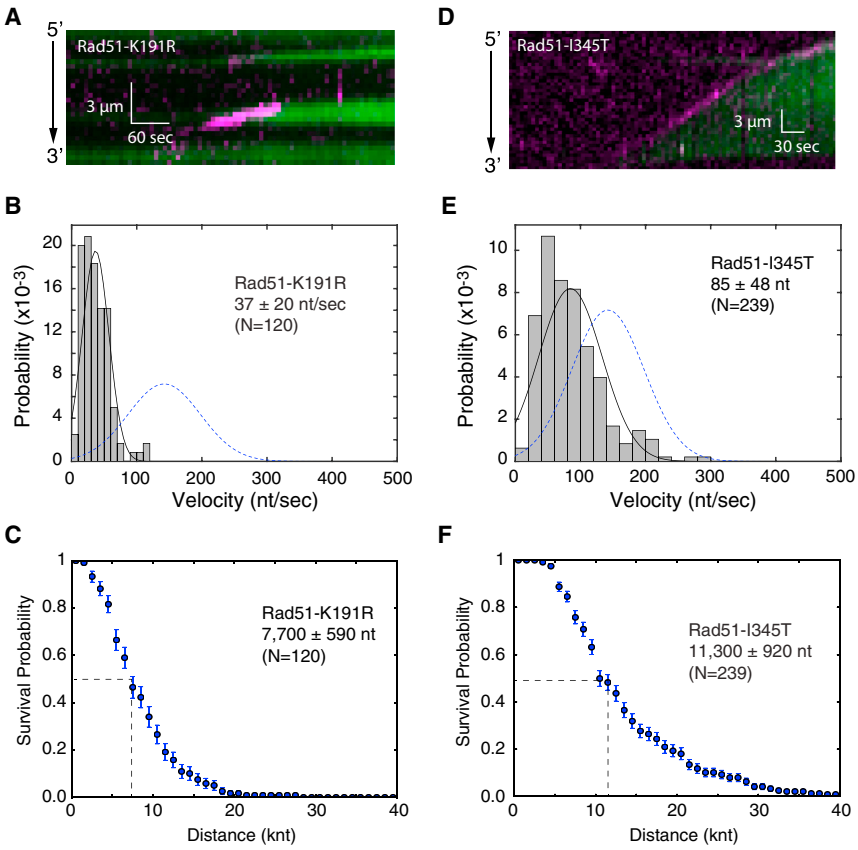

Figure 5. Rad51 Mutations that Restrict Clearance by Srs2

(A–C) Kymograph (A), velocity distribution (B), and survival probability analysis (C) for mCherry-Srs2^{898} translocation on presynaptic complexes prepared with Rad51-K191R.

(D–F) Kymograph (D), velocity distribution (E), and survival probability analysis (F) for mCherry-Srs2^{898} translocation on presynaptic complexes prepared with Rad51-I345T.

Error bars for the survival probability plots represent SD calculated by bootstrap analysis. The velocity distributions in (B) and (E) are superimposed on the Gaussian fit (blue dashed line) for the velocity distribution of unlabeled Srs2 taken from Figure 1E.

Srs2^{860}, revealing translocation and processivity values of 107 ± 63 nt/s and 13,000 ± 380 nt (n = 193), respectively (Figures 4D–4F; Table S1). Together, these findings suggest that truncating the Srs2 C-terminal domain markedly reduces the number of initial binding events, but once bound, the core SF1 helicase domain of Srs2 retains the ability to disrupt Rad51 filaments, albeit as a reduced velocity relative to Srs2^{898}. Taken together, these results indicate that the Rad51 interaction domain in Srs2 is not necessary for Rad51 filament disruption. These findings also imply that amino acids located within the C-terminal region of Srs2 help promote its association with the presynaptic complex.

Disruption of Human Rad51 by Yeast Srs2

We next asked whether *S. cerevisiae* Srs2 could clear human RAD51 from ssDNA. If species-specific contacts were necessary for Rad51 clearance from DNA, then yeast Srs2 should not be able to dismantle filaments of human RAD51. We found no evidence for disruption of the human RAD51 filaments under the same conditions (i.e., 100 pM Srs2) in which *S. cerevisiae* Rad51 was efficiently removed from the ssDNA. However, *S. cerevisiae* Srs2 is capable of removing human RAD51 from ssDNA at a Srs2 concentration (1 nM) that is 10 times greater than used in experiments with *S. cerevisiae* Rad51 (Figure 4G). When clearance of human RAD51 was evident, Srs2 exhibited a translocation velocity of 80 ± 40 nt/s and an average processivity of 6,400 ± 540 nt (n = 101) while clearing human RAD51 (Figures 4H and 4I; Table S1). In addition, these Srs2 complexes where much brighter than observed in experiments with *S. cerevisiae* Rad51, and it was evident that this increase in signal intensity was the consequence of multiple trailing Srs2 complexes moving rapidly along the RPA-ssDNA and then merging with the slower Srs2 ensembles positioned at the receding 3′ edge of the human RAD51 filaments (Figure 4G). We conclude that species-specific protein-protein contacts help promote efficient Srs2-mediated removal of Rad51 from ssDNA but are not an absolute requirement in this regard.

Rad51 ATP Hydrolysis Is Required for Efficient Srs2 Activity

The mutation of the lysine residue in the Walker A box of yeast Rad51 (Rad51^{K191R}) ablates DNA-dependent ATP hydrolysis activity and engenders sensitivity to certain DNA damaging agents (Fung et al., 2006; Morrison et al., 1999; Shinohara et al., 1992; Sung and Stratton, 1996). However, the Rad51^{K191R} mutant protein still binds to ssDNA and promotes DNA strand exchange (Fung et al., 2006; Morrison et al., 1999; Sung and Stratton, 1996). Previous bulk biochemical analysis has suggested that Srs2 is not as capable of removing Rad51^{K191R} from ssDNA (Antony et al., 2009). Interestingly, Rad51^{K191R} is not efficiently recruited to DNA breaks, but this deficiency is suppressed by the srs2Δ mutation, suggesting that Srs2 may remove Rad51^{K191R} from ssDNA *in vivo* (Fung et al., 2006). We asked whether Srs2 could remove Rad51^{K191R} from ssDNA in our assays. We approached this problem by first assessing the assembly and disassembly properties of Rad51^{K191R}. These results showed that although Rad51^{K191R} is compromised for filament assembly, it also dissociated from the ssDNA ~2.5-fold more slowly than WT Rad51 (Figure S4). Importantly, Srs2 was able to remove Rad51^{K191R} from ssDNA (Figure 5A) but translocated at just 36 ± 20 nt/s and exhibited a processivity of 7,700 ± 590 nt (n = 120) while moving along the Rad51^{K191R}-ssDNA filaments

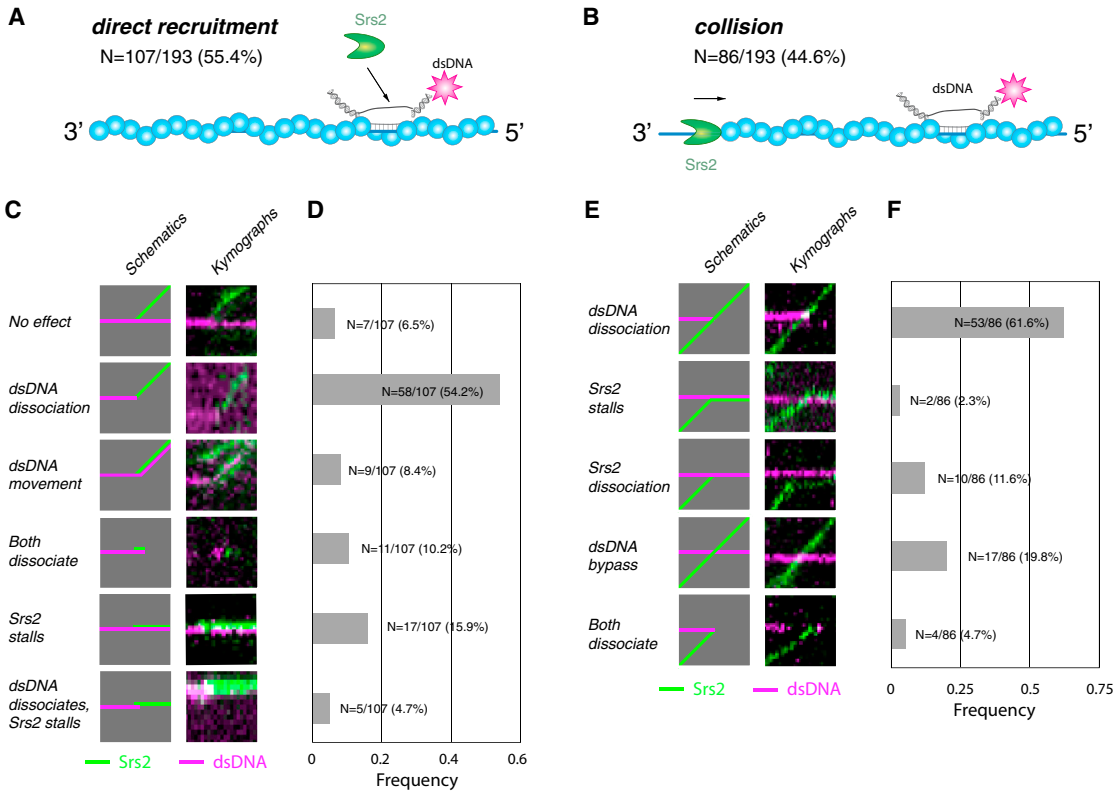

Figure 6. Srs2 Disruption of Heteroduplex DNA Joints

(A and B) Illustration showing two pathways for Srs2 interactions with the bound dsDNA fragments through either (A) direct recruitment or (B) collision events.

(C) Schematic illustrations and kymographs depicting the observed outcomes of Srs2 interactions involving direct binding to the dsDNA fragments.

(D) Relative frequency of each direct binding outcome.

(E) Schematic illustrations and kymographs depicting the observed outcomes of Srs2 interactions involving collisions with the dsDNA fragments.

(F) Relative frequency of each collision outcome.

(Figures 5B and 5C; Table S1). This ~75% reduction of the translocation velocity is quite striking and provides clear evidence for enhanced resistance of the Rad51^{K191R} filament to Srs2.

Rad51 Suppressor Mutations of rad55/57 Are Resistant to Srs2 Disruption

The stability of the Rad51 presynaptic filament is modulated by a balance between the stabilizing function of Rad55-Rad57 and the destabilizing function of Srs2 (Liu et al., 2011). Interestingly, Rad51^{I345T} was isolated as a suppressor mutation that partially bypasses the requirement for Rad55-Rad57, suggesting that the Rad51^{I345T} presynaptic complex might be more resistant to Srs2 (Fortin and Symington, 2002). We therefore examined the ability of Srs2 to disrupt presynaptic complexes prepared with Rad51^{I345T}. These experiments revealed that Srs2 is able to remove Rad51^{I345T} from ssDNA (Figure 5D), albeit more slowly than observed with WT Rad51, revealing velocity and processivity values of 85 ± 48 nt/s and 11,300 ± 920 nt (n = 239) (Figures 5E and 5F; Table S1). In agreement with previous findings (Malik and Symington, 2008), Rad51^{I345T} assembled more rapidly into filaments on ssDNA compared with WT Rad51 and also displayed a delayed in filament disassembly when chased with buffer lacking ATP (Figure S4). Together, these findings suggest that Rad51^{I345T} may overcome the genetic requirement for Rad55-Rad57 because of an increased affinity for ssDNA, which in turn lowers Srs2 velocity and processivity.

Srs2-Mediated Disruption of Heteroduplex DNA Joints

We have previously established assays for observing interactions between the Rad51 presynaptic complexes and short (70 bp) dsDNA substrates (Lee et al., 2015; Qi et al., 2015). We next asked whether Srs2 could process nucleoprotein intermediates that harbor ATTO 565-labeled dsDNA substrates bearing 15 nt of homology to the ssDNA that is bound by Rad51 (Lee et al., 2015; Qi et al., 2015). The fluorescently tagged dsDNA substrates were pre-incubated with the Rad51 filaments, and then GFP-Srs2 was injected into the sample chamber to determine its impact upon the fluorescent dsDNA molecules. Under these conditions, the dsDNA substrates undergo homologous pairing to form a paranemic joint that resembles a D-loop in structure (Figure 6A).

Srs2 interactions with these short dsDNA substrates could be segregated into two classes: (1) collision events involving translocation of Srs2 along the Rad51-ssDNA presynaptic complex until the DNA joints were encountered (Figure 6B) and (2) direct recruitment events in which Srs2 appeared to bind directly to

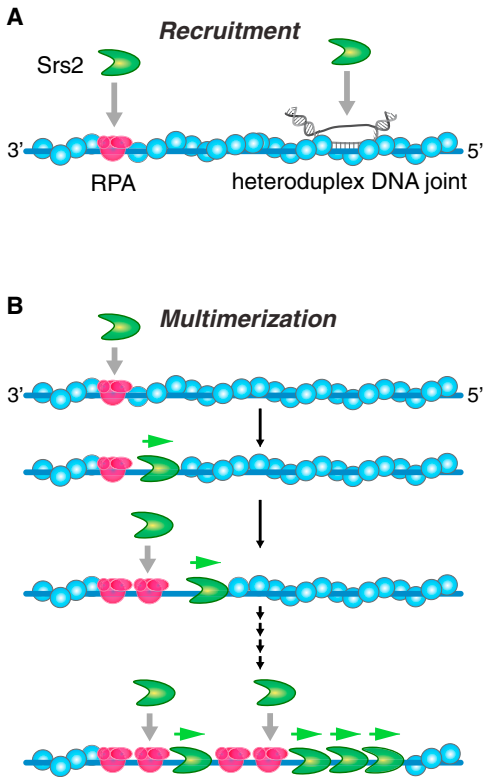

Figure 7. Models for the Recruitment and Formation of Tandem Srs2 Ensembles

(A) Illustration depicting Srs2 recruitment to the presynaptic complex through embedded clusters of RPA or bound dsDNA molecules.

(B) Proposed model for the formation of tandem ensembles of Srs2.

Details are presented in the main text.

the DNA joint (Figure 6A). Direct recruitment was the most common outcome for both substrates, accounting for ~55% of all interactions between Srs2 and the bound dsDNA substrates (Figure 6A). The most common outcomes for the direct recruitment events were the rapid dissociation of the dsDNA substrates, followed by continued Srs2 translocation along the presynaptic complex (54.2% [n = 58 of 107 events]) (Figures 6C and 6D). We also observed other types of less common events when Srs2 was directly recruited to the D-loops, including Srs2 stalling with concomitant displacement of the dsDNA (15.9% [n = 17 of 107]), dissociation of both Srs2 and the dsDNA (10.2% [n = 11 of 107]), and examples in which the dsDNA appeared to move with Srs2 (8.4% [n = 9 of 107]) (Figures 6C and 6D). Finally, a small fraction of the events assigned as direct recruitment had no effect on the dsDNA, and Srs2 continued translocation toward the 5′ ends of the ssDNA (6.5% [n = 7 of 107]) (Figures 6C and 6D). One possible explanation in these later cases was that Srs2 was unable to unwind the DNA joint sufficiently to allow it to dissociate from the presynaptic complexes, and these events may be mechanistically related to what takes place when Srs2 bypasses a bound dsDNA. Alternatively, Srs2 may have been recruited near the dsDNA but did not actually interact with the dsDNA itself.

Collison events accounted for ~45% of all observed interactions between Srs2 and the dsDNA bound to the Rad51-ssDNA presynaptic complexes. The most common outcome for these collision events was rapid displacement of the dsDNA from the presynaptic complex, followed by continued movement of Srs2 along the presynaptic complex (61.6% [n = 53 of 86]) (Figures 6E and 6F). In addition to dsDNA dissociation, we also observed instances in which Srs2 stalled or dissociated upon encountering the dsDNA (2.3% [n = 2 of 86] and 11.6% [n = 10 of 86], respectively) (Figures 6E and 6F). In addition, a significant fraction of the collisions resulted in Srs2 bypassing the dsDNA (19.8% [n = 17 of 86]) (Figures 6E and 6F). Because the ssDNA itself is not labeled, one explanation for these apparent bypass events may be that Srs2 was bound one of two overlapping ssDNA molecules. If this is the case, then our reported value (61.6%) for dsDNA dissociation during the collision events would represent a lower bound for the Srs2-mediated disruption of the dsDNA during the collisions events. Taken together, we conclude that Srs2 can readily remove short dsDNA fragments that are bound to the Rad51-ssDNA presynaptic complex and can do so through either direct recruitment to the heteroduplex DNA joint or by colliding with the heteroduplex DNA after approaching from the 3′→5′.

DISCUSSION

Here, we have directly visualized *S. cerevisiae* Srs2 in real time as it translocates on ssDNA and dismantles the Rad51 presynaptic complex. Our experiments have yielded insights into how Srs2 is recruited to the presynaptic complex, demonstrated that processive disruption of the Rad51 presynaptic complex is mediated by tandem assemblies of Srs2, and also revealed that Srs2 is preferentially targeted to and disrupts short paranemic joint.

Mechanism of Srs2 Recruitment

Although it is established that Srs2 dismantles Rad51 filaments, it has remained unclear how Srs2 is recruited to the presynaptic complex and other HR intermediates (Antony et al., 2009; Krejci et al., 2003; Marini and Krejci, 2010; Niu and Klein, 2017; Qiu et al., 2013; Sasanuma et al., 2013; Vasianovich et al., 2017; Veaute et al., 2003). In this study, we provide evidence that Srs2 is preferentially recruited to small clusters of RPA that remain embedded within the Rad51 presynaptic complex. Our data suggests that the C terminus of Srs2 encompassing the Rad51 interaction domain is important for the initial recruitment of Srs2 to these clusters of RPA. Importantly, we have previously shown that this domain is also essential for efficient recruitment of Srs2 to RPA-coated ssDNA even when Rad51 is absent from the reactions (De Tullio et al., 2017). Given these results, we propose that Srs2 is directly recruited to the RPA clusters embedded between Rad51 filaments, rather than Rad51 itself. An important implication of this finding is that as Srs2 begins stripping Rad51 from ssDNA, the newly created RPA-ssDNA that forms behind the leading Srs2 complex becomes available for the recruitment of additional Srs2 molecules (Figure 7). We have previously shown that Srs2 can strip RPA from the ssDNA,

and new Srs2 recruitment events take place even more readily on the newly cleared naked ssDNA (De Tullio et al., 2017). Thus, the recruitment mechanism may consist of interactions with RPA, ssDNA, or both.

The findings presented here also suggest that Srs2 may be specifically excluded from internal locations within the Rad51 filaments. Although Srs2 is known to physically interact with Rad51, it is not yet known where these contacts reside. If the Srs2 interacting surface were exposed on the surface of the Rad51 presynaptic complex, then one might expect Srs2 recruitment to take place uniformly within the Rad51 filaments. However, the finding that Srs2 preferentially associates with RPA clusters between Rad51 filaments suggests that the Srs2 interaction surface may reside between Rad51 monomers. We anticipate that this interaction surface may be normally buried between monomers within the Rad51 filaments, which would prevent Srs2 from randomly binding to any position within the Rad51 filament and instead confine it to interactions with the ends of the Rad51 filaments. Given that Srs2 translocates in the 3′→5′ direction, we propose that it is positioned to contact the protein surface of Rad51 that is oriented toward the 3′ end of the ssDNA (Figure 7). Our model therefore posits that the access of Srs2 is restricted to the 3′ end of the Rad51 filament. Within this context, the negative regulators of Srs2, which include the Rad55/57 complex, the SHU complex, and Rad52, may act by limiting access of Srs2 to the 3′ end of the Rad51 presynaptic complex.

Role of Tandem Srs2 Assemblies in Processive Rad51 Filament Disruption

The functional oligomeric states of DNA helicases have proved remarkably difficult to determine (Lohman et al., 2008). In many cases, there is evidence that helicases can behave as tandem assemblies while acting upon nucleic acids and that the changes in their oligomeric state regulate their activities (Lohman et al., 2008). Specific examples of tandem helicase assemblies include the bacteriophage T4 SF1 helicase DdaA (Byrd and Raney, 2004), the hepatitis C virus Sf2 helicase NS3 (Levin et al., 2004), and *E. coli* RecQ (Rad et al., 2015). In addition, recent studies have shown that *E. coli* UvrD translocates either as a monomer or as two tandem monomers, and that the tandem monomers are more processive than a single monomer (Comstock et al., 2015; Lee et al., 2013). Similarly, recent biochemical results have suggested that more than one Srs2 monomer is required for efficient DNA unwinding (Lytle et al., 2014). Our work now demonstrates that processive disruption of Rad51 filaments involves multiple Srs2 molecules acting upon the same filament end. This conclusion is also consistent with electron microscopy images of Srs2 on Rad51-ssDNA, which revealed Srs2 species that are oligomeric in structure (Dupaigne et al., 2008). We propose a model to explain how tandem assemblies of Srs2 act to dissociate Rad51 from ssDNA (Figure 7). We propose that Srs2-dependent removal of Rad51 from the ssDNA lead to new tracts of RPA-ssDNA or near naked ssDNA, which can then function as loading sites for additional Srs2 molecules. Separate measurements indicate that Srs2 translocates on RPA-ssDNA at a rate that is ~20% faster than that on Rad51-ssDNA and travels even faster on naked ssDNA (De Tullio et al., 2017). The ability of Srs2 to translocate more rapidly on RPA-ssDNA would allow any newly loaded Srs2 molecules to quickly catch up to and merge with the leading Srs2 ensemble already present at the receding 3′ edge of the Rad51 filament. It should be noted that although our work shows that tandem assemblies of Srs2 are involved in processive disruption of Rad51 filaments *in vitro*, we do not know the oligomeric state of Srs2 *in vivo*. Similarly, do not know how Srs2 will behave on native presynaptic complexes, which contain many other RAD52 group proteins in addition to Rad51 (e.g., Rad52, Rad55/57, Rad54, Rdh54, the SHU complex) (Heyer et al., 2010; Kowalczykowski, 2015; Symington et al., 2014). It remains unknown how Srs2 will behave on these more complex, multi-protein assemblies, but Rad52, Rad55/57 and the SHU complex have all been implicated as potential regulators of Srs2 activities (Bernstein et al., 2011; Burgess et al., 2009; Liu et al., 2011).

Srs2 translocation has been examined by bulk biochemical and single molecule fluorescence resonance energy transfer (FRET) assays (Antony et al., 2009; Qiu et al., 2013). Results from these studies have suggested that Srs2 remains monomeric while acting on its substrates, translocating at ~300 nt/s over an estimated distance of ~1,500 nt and removing Rad51 at a rate of ~12 monomers/s, corresponding to ~36 nt/s (Antony et al., 2009). In contrast, our results suggest that arrays Srs2 multimers can translocate over remarkably long distances (~18,000 nt) on Rad51-ssDNA while traveling at an apparent velocity of ~140 nt/s, corresponding to the disruption of ~6,000 Rad51 monomers at a rate of ~50 monomers/s. We attribute the differences between our findings and the published results to the use of much longer ssDNA substrates and the inclusion of free RPA in our study, thus enhancing assembly of the tandem Srs2 ensembles that possess greater processivity and velocity.

Srs2 Is Directly Recruited to Heteroduplex DNA Joints

Genetic and biochemical studies have implicated Srs2 in disrupting strand invasion intermediates such as D-loops and extended D-loops (Heyer et al., 2010; Ira et al., 2003; Liu et al., 2017). The ability of Srs2 to disrupt these structures is thought to play two important roles during HR. First, Srs2 dismantles inappropriate intermediates, some proportion of which may be composed of D-loops. Second, Srs2-mediated heteroduplex DNA disruption promotes synthesis-dependent strand annealing (SDSA) and in doing so suppresses the formation of crossover recombination products, which is important to prevent loss of heterozygosity and chromosomal rearrangements. These studies raise the question of how Srs2 is targeted to strand invasion intermediates. Our findings show that Srs2 can engage dsDNA paired with the Rad51-ssDNA presynaptic complex by either translocating along the Rad51-ssDNA until encountering the DNA joint or binding to the heteroduplex DNA joint directly. Indeed, our finding that more than half of all observed Srs2 recruitment at sites of Rad51-filament bound dsDNA is especially notable given that there were only about three to five dsDNA fragments bound per ~35,000 nt of presynaptic ssDNA, which would correspond to ≤2% of the total available DNA present (Lee et al., 2015; Qi et al., 2015). These considerations highlight the strong enrichment for Srs2 binding interactions with the bound dsDNA molecules compared with the remaining portions

of the presynaptic complex, and support a model in which Srs2 is directly recruited to Rad51-generated heteroduplex DNA joints (Figure 7).

Conclusions

Here, we have established methods for examining antirecombinases in real time as they act on long ssDNA substrates mimicking early HR intermediates, and these experiments have provided insights into the action of Srs2 on the Rad51 presynaptic complex. Other helicases, such as yeast Mph1 and mammalian FBH1, RECQ5, and RTEL1, have been implicated in the regulation of HR either via disruption of the Rad51 presynaptic filament or strand invasion intermediates (Branzei and Szakal, 2017; Brosh, 2013; Symington and Heyer, 2006). However, we have only a rudimentary understanding of how Srs2, and other regulators of HR act to prevent the formation of aberrant recombination intermediates. Moreover, Rad52, Rad55/57, and the SHU complex have all been implicated in the negative regulation of Srs2 activity (Bernstein et al., 2011; Burgess et al., 2009; Liu et al., 2011). Future studies using our single-molecule assays will likely shed light on the mechanisms of antirecombinases and how the activities of these DNA motor proteins are regulated by the aforementioned factors and their orthologs in other eukaryotes.

EXPERIMENTAL PROCEDURES

Proteins

S. cerevisiae Rad51, RPA, GFP-RPA, and mCherry-RPA were purified as described (Gibb et al., 2014; Qi et al., 2015). pET11d vectors encoding 9xHis-tagged Srs2, GFP-Srs2^{898}, mCherry-Srs2^{898}, GFP-Srs2^{860}, Srs2^{K41A}, Srs2$^{K41A:898}$, and Srs2$^{\Delta875–902}$ were expressed *E. coli* Rosetta2 (DE3) cells (Novagen), and the proteins were purified as described (De Tullio et al., 2017).

Single-Molecule Imaging

All experiments were conducted with a custom-built prism-type total internal reflection fluorescence (TIRF) microscope (Nikon) equipped with a 488 nm laser (Coherent Sapphire, 200 mW) and a 561 nm laser (Coherent Sapphire, 200 mW) (De Tullio et al., 2017). Flow cells and ssDNA curtains were prepared as described (Ma et al., 2017). In brief, lipid bilayers were prepared with 91.5% DOPC, 0.5% biotinylated-DPPE, and 8% mPEG 2000-DOPE. The ssDNA substrate was generated using a biotinylated primer annealed to a circular M13 ssDNA template and rolling circle replication. Biotinylated ssDNA was injected into the sample chamber and attached to the bilayer through a biotin-streptavidin linkage. Buffer was delivered to the sample chambers using a syringe pump (Kd Scientific), and sample delivery was controlled by two SCIVEX HPLC valves equipped with 150 μL loops. The ssDNA was aligned at the barriers by application of flow in HR buffer (30 mM Tris-Ac [pH 7.5], 50 mM KCl, 5 mM MgAc, 1 mM DTT, and 0.3 mg/mL BSA) at 0.8 mL/min. Secondary structure was reduced with 150 μL of 4 M urea in 30 mM Tris-HCl (pH 7.4), immediately followed by 0.1–3 mL of HR buffer containing 10–5,000 pM unlabeled RPA, GFP-RPA, or mCherry-RPA, as indicated. Rad51 filament formation was initiated by injecting HR buffer containing 2 mM ATP and 1–2 μM Rad51, followed by a 10–15 min incubation in the absence of buffer flow. Flow was resumed with HR buffer containing 2 mM ATP and 100 pM RPA at 0.2 mL/min for 3 min to flush any remaining Rad51. Srs2 was injected through a 150 μL sample loop, and activity was observed under constant flow of HR buffer containing 2 mM ATP and 100 pM RPA. Upon completion of the experiments, the presence of any remaining active Rad51-ssDNA filaments after 15–30 min of Srs2 activity was confirmed by flushing the sample chamber with GFP-RPA or mCherry-RPA in HR buffer that lacked ATP.

SUPPLEMENTAL INFORMATION

Supplemental Information includes Supplemental Experimental Procedures, four figures, one table, and four movies and can be found with this article online at https://doi.org/10.1016/j.celrep.2017.11.047.

ACKNOWLEDGMENTS

We thank Rodney Rothstein, Lorraine Symington, and members of the Greene laboratory for their advice throughout this work. With thank J. Brooks Crickard for comments on the manuscript and Tsuyoshi Terakawa for assistance with data analysis. This research was funded by NIH grants to E.C.G. (R35GM118026) and P.S. (R01ES007061 and R01ES015632). L.D.T. was funded by a PEW Latin American postdoctoral fellowship (Grant No. 27354), the Williams Foundation, and a program for Assistant Researchers, CONICET, Argentina.

AUTHOR CONTRIBUTIONS

K.K. designed and conducted the single-molecule experiments and data analysis with assistance from L.D.T. B.G. established the initial DNA curtain assays for Srs2. Y.K. expressed and purified Rad51 and Dmc1. E.C.G. supervised the project and wrote the manuscript with input from K.K., L.D.T., B.G., Y.K., and P.S.

DECLARATION OF INTERESTS

The authors declare no competing interests.

Received: September 13, 2017
Revised: October 22, 2017
Accepted: November 13, 2017
Published: December 12, 2017

REFERENCES

Antony, E., Tomko, E.J., Xiao, Q., Krejci, L., Lohman, T.M., and Ellenberger, T. (2009). Srs2 disassembles Rad51 filaments by a protein-protein interaction triggering ATP turnover and dissociation of Rad51 from DNA. Mol. Cell *35*, 105–115.

Bernstein, K.A., Gangloff, S., and Rothstein, R. (2010). The RecQ DNA helicases in DNA repair. Annu. Rev. Genet. *44*, 393–417.

Bernstein, K.A., Reid, R.J., Sunjevaric, I., Demuth, K., Burgess, R.C., and Rothstein, R. (2011). The Shu complex, which contains Rad51 paralogues, promotes DNA repair through inhibition of the Srs2 anti-recombinase. Mol. Biol. Cell *22*, 1599–1607.

Branzei, D., and Szakal, B. (2017). Building up and breaking down: mechanisms controlling recombination during replication. Crit. Rev. Biochem. Mol. Biol. *52*, 381–394.

Brosh, R.M., Jr. (2013). DNA helicases involved in DNA repair and their roles in cancer. Nat. Rev. Cancer *13*, 542–558.

Burgess, R.C., Lisby, M., Altmannova, V., Krejci, L., Sung, P., and Rothstein, R. (2009). Localization of recombination proteins and Srs2 reveals anti-recombinase function in vivo. J. Cell Biol. *185*, 969–981.

Byrd, A.K., and Raney, K.D. (2004). Protein displacement by an assembly of helicase molecules aligned along single-stranded DNA. Nat. Struct. Mol. Biol. *11*, 531–538.

Chen, R., and Wold, M.S. (2014). Replication protein A: single-stranded DNA's first responder: dynamic DNA-interactions allow replication protein A to direct single-strand DNA intermediates into different pathways for synthesis or repair. BioEssays *36*, 1156–1161.

Colavito, S., Macris-Kiss, M., Seong, C., Gleeson, O., Greene, E.C., Klein, H.L., Krejci, L., and Sung, P. (2009). Functional significance of the Rad51-Srs2 complex in Rad51 presynaptic filament disruption. Nucleic Acids Res. *37*, 6754–6764.

Comstock, M.J., Whitley, K.D., Jia, H., Sokoloski, J., Lohman, T.M., Ha, T., and Chemla, Y.R. (2015). Protein structure. Direct observation of structure-function relationship in a nucleic acid-processing enzyme. Science *348*, 352–354.

De Tullio, L., Kaniecki, K., Kwon, Y., Crickard, J.B., Sung, P., and Greene, E.C. (2017). Yeast Srs2 helicase promotes redistribution of single-stranded DNA-bound RPA and Rad52 in homologous recombination regulation. Cell Rep. *21*, 570–577.

Dupaigne, P., Le Breton, C., Fabre, F., Gangloff, S., Le Cam, E., and Veaute, X. (2008). The Srs2 helicase activity is stimulated by Rad51 filaments on dsDNA: implications for crossover incidence during mitotic recombination. Mol. Cell *29*, 243–254.

Fortin, G.S., and Symington, L.S. (2002). Mutations in yeast Rad51 that partially bypass the requirement for Rad55 and Rad57 in DNA repair by increasing the stability of Rad51-DNA complexes. EMBO J. *21*, 3160–3170.

Fung, C.W., Fortin, G.S., Peterson, S.E., and Symington, L.S. (2006). The rad51-K191R ATPase-defective mutant is impaired for presynaptic filament formation. Mol. Cell. Biol. *26*, 9544–9554.

Gibb, B., Ye, L.F., Kwon, Y., Niu, H., Sung, P., and Greene, E.C. (2014). Protein dynamics during presynaptic-complex assembly on individual single-stranded DNA molecules. Nat. Struct. Mol. Biol. *21*, 893–900.

Heyer, W.D., Ehmsen, K.T., and Liu, J. (2010). Regulation of homologous recombination in eukaryotes. Annu. Rev. Genet. *44*, 113–139.

Hunter, N. (2015). Meiotic recombination: the essence of heredity. Cold Spring Harb. Perspect. Biol. *7*, 7.

Ira, G., Malkova, A., Liberi, G., Foiani, M., and Haber, J.E. (2003). Srs2 and Sgs1-Top3 suppress crossovers during double-strand break repair in yeast. Cell *115*, 401–411.

Klein, H.L. (2001). Mutations in recombinational repair and in checkpoint control genes suppress the lethal combination of srs2Delta with other DNA repair genes in Saccharomyces cerevisiae. Genetics *157*, 557–565.

Kowalczykowski, S.C. (2015). An overview of the molecular mechanisms of recombinational DNA repair. Cold Spring Harb. Perspect. Biol. *7*, 7.

Krejci, L., Van Komen, S., Li, Y., Villemain, J., Reddy, M.S., Klein, H., Ellenberger, T., and Sung, P. (2003). DNA helicase Srs2 disrupts the Rad51 presynaptic filament. Nature *423*, 305–309.

Krejci, L., Macris, M., Li, Y., Van Komen, S., Villemain, J., Ellenberger, T., Klein, H., and Sung, P. (2004). Role of ATP hydrolysis in the antirecombinase function of Saccharomyces cerevisiae Srs2 protein. J. Biol. Chem. *279*, 23193–23199.

Lee, K.S., Balci, H., Jia, H., Lohman, T.M., and Ha, T. (2013). Direct imaging of single UvrD helicase dynamics on long single-stranded DNA. Nat. Commun. *4*, 1878.

Lee, J.Y., Terakawa, T., Qi, Z., Steinfeld, J.B., Redding, S., Kwon, Y., Gaines, W.A., Zhao, W., Sung, P., and Greene, E.C. (2015). DNA recombination. Base triplet stepping by the Rad51/RecA family of recombinases. Science *349*, 977–981.

Levin, M.K., Wang, Y.H., and Patel, S.S. (2004). The functional interaction of the hepatitis C virus helicase molecules is responsible for unwinding processivity. J. Biol. Chem. *279*, 26005–26012.

Liu, J., Renault, L., Veaute, X., Fabre, F., Stahlberg, H., and Heyer, W.D. (2011). Rad51 paralogues Rad55-Rad57 balance the antirecombinase Srs2 in Rad51 filament formation. Nature *479*, 245–248.

Liu, J., Ede, C., Wright, W.D., Gore, S.K., Jenkins, S.S., Freudenthal, B.D., Todd Washington, M., Veaute, X., and Heyer, W.D. (2017). Srs2 promotes synthesis-dependent strand annealing by disrupting DNA polymerase δ-extending D-loops. eLife *6*, 6.

Lohman, T.M., Tomko, E.J., and Wu, C.G. (2008). Non-hexameric DNA helicases and translocases: mechanisms and regulation. Nat. Rev. Mol. Cell Biol. *9*, 391–401.

Lytle, A.K., Origanti, S.S., Qiu, Y., VonGermeten, J., Myong, S., and Antony, E. (2014). Context-dependent remodeling of Rad51-DNA complexes by Srs2 is mediated by a specific protein-protein interaction. J. Mol. Biol. *426*, 1883–1897.

Ma, C.J., Steinfeld, J.B., and Greene, E.C. (2017). Single-stranded DNA curtains for studying homologous recombination. Methods Enzymol. *582*, 193–219.

Malik, P.S., and Symington, L.S. (2008). Rad51 gain-of-function mutants that exhibit high affinity DNA binding cause DNA damage sensitivity in the absence of Srs2. Nucleic Acids Res. *36*, 6504–6510.

Marini, V., and Krejci, L. (2010). Srs2: the "odd-job man" in DNA repair. DNA Repair (Amst.) *9*, 268–275.

Mehta, A., and Haber, J.E. (2014). Sources of DNA double-strand breaks and models of recombinational DNA repair. Cold Spring Harb. Perspect. Biol. *6*, a016428.

Morrison, C., Shinohara, A., Sonoda, E., Yamaguchi-Iwai, Y., Takata, M., Weichselbaum, R.R., and Takeda, S. (1999). The essential functions of human Rad51 are independent of ATP hydrolysis. Mol. Cell. Biol. *19*, 6891–6897.

Niu, H., and Klein, H.L. (2017). Multifunctional roles of Saccharomyces cerevisiae Srs2 protein in replication, recombination and repair. FEMS Yeast Res. *17* (2).

Pâques, F., and Haber, J.E. (1999). Multiple pathways of recombination induced by double-strand breaks in Saccharomyces cerevisiae. Microbiol. Mol. Biol. Rev. *63*, 349–404.

Qi, Z., Redding, S., Lee, J.Y., Gibb, B., Kwon, Y., Niu, H., Gaines, W.A., Sung, P., and Greene, E.C. (2015). DNA sequence alignment by microhomology sampling during homologous recombination. Cell *160*, 856–869.

Qiu, Y., Antony, E., Doganay, S., Koh, H.R., Lohman, T.M., and Myong, S. (2013). Srs2 prevents Rad51 filament formation by repetitive motion on DNA. Nat. Commun. *4*, 2281.

Rad, B., Forget, A.L., Baskin, R.J., and Kowalczykowski, S.C. (2015). Single-molecule visualization of RecQ helicase reveals DNA melting, nucleation, and assembly are required for processive DNA unwinding. Proc. Natl. Acad. Sci. USA *112*, E6852–E6861.

Sasanuma, H., Furihata, Y., Shinohara, M., and Shinohara, A. (2013). Remodeling of the Rad51 DNA strand-exchange protein by the Srs2 helicase. Genetics *194*, 859–872.

Shinohara, A., Ogawa, H., and Ogawa, T. (1992). Rad51 protein involved in repair and recombination in S. cerevisiae is a RecA-like protein. Cell *69*, 457–470.

Simandlova, J., Zagelbaum, J., Payne, M.J., Chu, W.K., Shevelev, I., Hanada, K., Chatterjee, S., Reid, D.A., Liu, Y., Janscak, P., et al. (2013). FBH1 helicase disrupts RAD51 filaments in vitro and modulates homologous recombination in mammalian cells. J. Biol. Chem. *288*, 34168–34180.

Sung, P., and Stratton, S.A. (1996). Yeast Rad51 recombinase mediates polar DNA strand exchange in the absence of ATP hydrolysis. J. Biol. Chem. *271*, 27983–27986.

Symington, L.S., and Heyer, W.D. (2006). Some disassembly required: role of DNA translocases in the disruption of recombination intermediates and dead-end complexes. Genes Dev. *20*, 2479–2486.

Symington, L.S., Rothstein, R., and Lisby, M. (2014). Mechanisms and regulation of mitotic recombination in Saccharomyces cerevisiae. Genetics *198*, 795–835.

Vasianovich, Y., Altmannova, V., Kotenko, O., Newton, M.D., Krejci, L., and Makovets, S. (2017). Unloading of homologous recombination factors is required for restoring double-stranded DNA at damage repair loci. EMBO J. *36*, 213–231.

Veaute, X., Jeusset, J., Soustelle, C., Kowalczykowski, S.C., Le Cam, E., and Fabre, F. (2003). The Srs2 helicase prevents recombination by disrupting Rad51 nucleoprotein filaments. Nature *423*, 309–312.